Scaling of discrete dislocation predictions for near-threshold fatigue crack growth

Deshpande, VS; Needleman, A; van der Giessen, Erik

Published in:
Acta Materialia

DOI:
10.1016/S1359-6454(03)00302-1

Publication date:
2003

Available online at www.sciencedirect.com
SCIENCE DIRECT®
Pergamon
Acta Materialia 51 (2003) 4637–4651
Acta MATERIALIA
www.actamat-journals.com

Scaling of discrete dislocation predictions for near-threshold fatigue crack growth

V.S. Deshpande [a], A. Needleman [b,*], E. Van der Giessen [c]

[a] *Department of Engineering, Cambridge University, Trumpington Street, Cambridge CB2 1PZ, UK*
[b] *Department of Engineering, Brown University, 182 Hope Street, Providence, RI 02912, USA*
[c] *Department of Applied Physics, University of Groningen, Nyenborgh 4, 9747 AG Groningen, The Netherlands*

Received 4 April 2003; received in revised form 4 April 2003; accepted 1 June 2003

Abstract

Analyses of the growth of a plane strain crack subject to remote mode I cyclic loading under small scale yielding are carried out using discrete dislocation dynamics. Plastic deformation is modelled through the motion of edge dislocations in an elastic solid with the lattice resistance to dislocation motion, dislocation nucleation, dislocation interaction with obstacles and dislocation annihilation being incorporated through a set of constitutive rules. An irreversible relation is specified between the opening traction and the displacement jump across a cohesive surface ahead of the initial crack tip in order to simulate cyclic loading in an oxidizing environment. Calculations are carried out with different material parameters so that values of yield strength, cohesive strength and elastic moduli varying by factors of three to four are considered. The fatigue crack growth predictions are found to be insensitive to the yield strength of the material despite the number of dislocations and the plastic zone size varying by approximately an order of magnitude. The fatigue threshold scales with the fracture toughness of the purely elastic solid, with the experimentally observed linear scaling with Young's modulus an outcome when the cohesive strength scales with Young's modulus.

Keywords: Dislocations; Mechanical properties; Fatigue; Plastic; Computer simulation

1. Introduction

Fatigue crack growth of long cracks in metals can generally be divided into three characteristic regimes [1] in order of increasing load amplitude; (A) a near-threshold regime where crack growth rates are of the order of the lattice spacing, (B) a power-law or Paris law [2] regime and (C) a rapid growth regime that is dominated by the monotonic fracture toughness K_{IC}. At least in the near-threshold and Paris law regimes, fatigue crack growth rates are relatively independent of the yield strength of the material but scale with the elastic modulus. This rather surprising observation has been borne out in numerous studies on a variety of metallic alloys including for example steels [3], copper [4] and aluminum [5]. Experimental data for the effective fatigue threshold ΔK_{th}^{eff} reported by Liaw et al. [5] and Hertzberg [6] indicates that

* Corresponding author. Tel.: +1-401-863-2863; fax: +1-401-863-9009.
E-mail address: needle@engin.brown.edu (A. Needleman).

1359-6454/03/$30.00
doi:10.1016/S1359-6454(03)00302-1

$(\Delta K_{th}^{eff}/E)^2 \approx b$, where b is the Burgers vector magnitude and E is the Young's modulus. The normalized effective fatigue threshold $\Delta K_{th}^{eff}/E$ for a variety of metallic alloys is plotted in Fig. 1 as a function of the normalized yield strength σ_Y/E from the data in Kang et al. [7]: ΔK_{th}^{eff} is seen to be reasonably independent of the yield strength over nearly two orders of magnitude variation in σ_Y/E.

A variety of continuum plasticity models have been proposed to rationalize the fatigue behavior in regimes (A) and (B). Usami and Shida [8] postulated that the fatigue threshold corresponds to a critical plastic zone size while Donahue et al. [9] proposed that the threshold for the onset of crack growth occurs when the crack tip opening displacement attains a value comparable to a critical microstructural parameter. Models for the Paris law regime include the geometric models of Laird and Smith [10] and of McClintock [11], which presume that crack growth rates are proportional to the crack tip opening displacement, and the damage accumulation models of Weertman [12] and Rice [13]. A feature of all these models is that they predict a dependence of the crack growth rates on the yield strength of the material in contrast to experimental observations. More recently, Nguyen et al. [14] and Tvergaard and Hutchinson [15] reported numerical calculations of fatigue crack growth in which the material was characterized by a conventional continuum plasticity model. While Nguyen et al. [14] embedded the fracture properties in a cohesive model with loading/unloading hysteresis, Tvergaard and Hutchinson [15] related the crack growth rate to the crack tip opening displacement. Undoubtedly, these models also predict a dependence of the fatigue crack growth rates on the yield strength of the material.

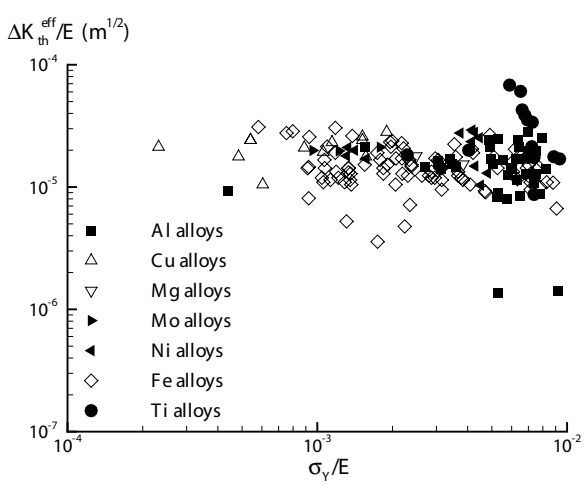

Fig. 1. Experimental values of ΔK_{th}^{eff} for a variety of metallic alloys showing that ΔK_{th}^{eff} is approximately independent of the yield strength σ_Y and scales approximately linearly with Young's modulus E. The data is replotted from that presented in Ref. [7].

Literature on dislocation models for fatigue has been reviewed by Riemelmoser et al. [16]. Dislocation models by Pippan et al. [17–19] and Wilkinson et al. [20], are meant to represent the deformation-controlled fatigue crack growth mechanism proposed by Laird and Smith [10] and Neumann [21]. They postulate the onset of fatigue crack growth when dislocations nucleate from the crack tip or a single source near the crack tip at some critical stress intensity factor k_{emit}. Using the Rice–Thomson [22] estimate for $k_{emit} \propto E\sqrt{b}$, these models predict that $\Delta K_{th} \propto E\sqrt{b}$.

Here, we analyze the scaling of the fatigue crack growth rates with the yield strength, Young's modulus and cohesive strength and energy in the near-threshold regime using the discrete dislocation plasticity framework used in previous studies to analyze the fatigue threshold [23], the Paris-law behavior of long cracks [24] and the accelerated growth rate of short cracks [25]. A key feature of the approach is that the material model and fracture properties are independent, with the material model applicable whether or not there is a crack, see e.g. Ref. [26]. The fracture properties are embedded in a cohesive surface constitutive relative and thus crack growth, which is stress as well as deformation driven, occurs as a natural outcome of the boundary value problem solution. As in Refs. [23,24], a plane strain small scale yielding boundary value problem is formulated and solved with plasticity occurring due to the motion of a large number of edge dislocations. Variations of Young's modulus E by a factor of four and of yield strength σ_Y by a factor of three are analyzed using the framework employed in Refs. [23,24]. The outcome of the boundary value problem solutions is

used to assess the scaling of the fatigue crack growth rates with E and σ_Y.

2. Discrete dislocation formulation

The plane strain small scale yielding problem analyzed is sketched in Fig. 2. The boundary value formulation is that of Van der Giessen and Needleman [27] where plastic flow arises from the collective motion of a large number of dislocations. The formulation is outlined here and further details and references are given in Refs. [23–25]. Geometry changes are neglected and symmetry about the crack plane is assumed. Remote from the crack tip, displacements corresponding to the linear elastic mode I K-field are applied, and crack initiation and growth are modelled using a cohesive surface framework, as in Ref. [28] with dislocation nucleation from the crack tip not explicitly modelled. For computational convenience, dislocation activity is restricted to a process window of dimensions $L_p \times h_p = 40 \times 40$ μm. Computations are terminated before any dislocations reach the boundary of the process window so that the effect of the process window is to restrict the loading range that can be analyzed. The analyses are two-dimensional, under plane strain, and the crystal is taken to have three slip systems, to mimic the ambiguity of slip that exists in three-dimensional fcc crystals. Two slip systems have their slip planes oriented at $\theta = \pm 60°$ from the crack plane and a third one at $\theta = 0°$. At any time t, the body is in equilibrium with the applied loads and displacements, and the position of each dislocation in the body is known. An increment of loading is applied and the stress and displacement fields, and the dislocation structure are determined at $t + \Delta t$.

The dislocations are treated as line singularities in an elastically isotropic continuum with Young's modulus E and Poisson's ratio ν. Unless otherwise stated, $E = 70$ GPa and $\nu = 0.33$. Consistent with the plane strain condition, only edge dislocations are considered, all having the same Burgers vector, $b = 0.25$ nm. The potentially active slip planes are spaced at $100b$.

The long range elastic interactions between dislocations are accounted for directly in the boundary value problem solution. Short range interactions enter through a set of constitutive rules of the type suggested by Kubin et al. [29]. Constitutive rules are specified for: (i) dislocation glide; (ii) annihil-

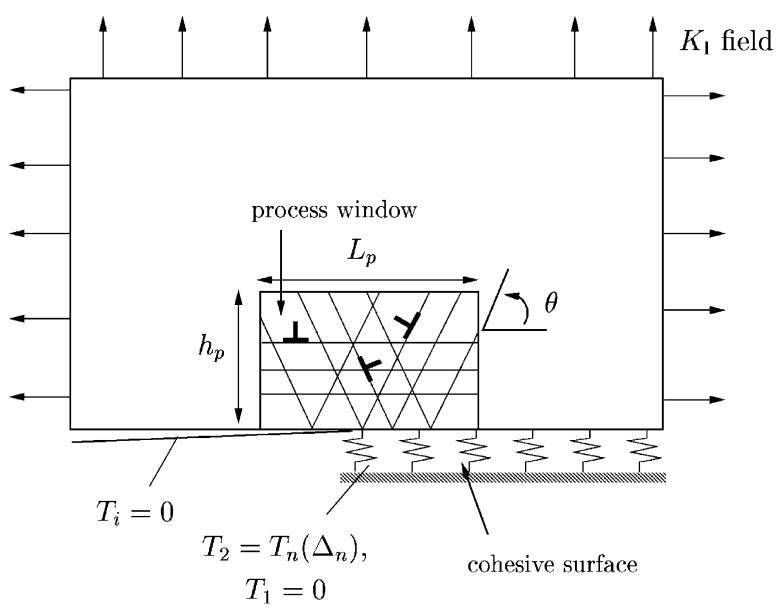

Fig. 2. Sketch of the small scale yielding boundary value problem analyzed.

ation; (iii) nucleation; (iv) obstacle pinning. The glide velocity is taken to be linearly related to the Peach–Koehler force with a drag coefficient $B = 10^{-4}$ Pa s, a representative value for several fcc crystals [29]. Dislocations of opposite sign annihilate when they come within a critical distance of $L_e = 6b$. Initially, the three slip systems are free of mobile dislocations, but dislocations can be generated from discrete sources that are randomly distributed with a density of 20/μm^2. These point sources mimic Frank-Read sources from pinned segments on out-of-plane slip systems which are not explicitly considered. They generate a dipole when the Peach–Koehler force exceeds a critical value of $\tau_{\text{nuc}}b$ during a period of time t_{nuc}, with $t_{\text{nuc}} = 10$ ns. The distance L_{nuc} between the opposite signed dislocations is taken to be specified by

$$L_{\text{nuc}} = \frac{E}{4\pi(1-\nu^2)}\frac{b}{\tau_{\text{nuc}}}. \tag{1}$$

This choice of L_{nuc} ensures that the shear stress of one dislocation acting on the other is balanced by the slip system shear stress τ_{nuc}. There is also a random distribution of 60 point obstacles per μm^2, which represent either small precipitates on the slip plane or forest dislocations on out-of-plane slip systems. The obstacles pin dislocations as long as the Peach–Koehier force is below the obstacle strength $b\tau_{\text{obs}}$. Calculations are carried out for four sets of nucleation and obstacle strengths: (i) $\tau_{\text{nuc}} = 50$ MPa and $\tau_{\text{obs}} = 150$ MPa; (ii) $\tau_{\text{nuc}} = 25$ MPa and $\tau_{\text{obs}} = 75$ MPa; (iii) $\tau_{\text{nuc}} = 20$ MPa and $\tau_{\text{obs}} = 60$ MPa; and (iv) $\tau_{\text{nuc}} = 15$ MPa and $\tau_{\text{obs}} = 45$ MPa. The materials are identical in all other respects including the spatial distribution of the sources and obstacles, but exhibit different yield strengths.

At each time step, the stress and displacement fields are obtained by superposition as described in Ref. [27]. The fields are written as

$$\sigma_{ij} = \tilde{\sigma}_{ij} + \hat{\sigma}_{ij}, \quad u_i = \tilde{u}_i + \hat{u}_i, \tag{2}$$

where the ($\tilde{}$)-fields are the singular fields associated with each individual dislocation, e.g.,

$$\tilde{\sigma}_{ij} = \sum_{I=1}^{N} \tilde{\sigma}_{ij}^{(I)},$$

where N is the number of dislocations and $\tilde{\sigma}_{ij}^{(I)}$ is the stress field associated with dislocation I in the half-space $x_2 \geq 0$. The ($\hat{}$)-fields are image fields that enforce the boundary conditions in either the displacements or the tractions $T_i = \sigma_{ij}n_j$ (n_j is the outward normal to the appropriate surface). The ($\hat{}$)-fields are smooth and are obtained by a finite element method. Resolving the dislocation dynamics requires a small time step of $\Delta t = 0.5$ ns. Thus, the calculations were carried out with a rather high loading rate of $\dot{K}_I = 100$ GPa$\sqrt{\text{m}}$/s in order to reduce the time required for the computations. The effect of loading rate is not explored here. However, in Ref. [30], under monotonic loading conditions, varying the loading rate by two orders of magnitude was not found to change the crack growth behavior qualitatively, although, of course, a strong tendency was found for increased plastic deformation at lower loading rates.

Along the cohesive surface, $T_1 = 0$ (from symmetry) while the magnitude of T_2 has the universal binding form [31],

$$T_2(\Delta_2) = \sigma_{\text{coh}}\frac{\Delta_2}{\delta_n}\exp\left(-\frac{\Delta_2}{\delta_n} + 1\right), \tag{3}$$

where $\Delta_2 = 2u_2(x_1,0)$ is the cohesive opening, σ_{coh} is the normal cohesive strength and δ_n is a characteristic length. For monotonic separation, the work of separation is given by $\phi_n = \exp(1)\,\sigma_{\text{coh}}\delta_n$ and is related to a reference stress intensity factor K_0 by

$$K_0 = \sqrt{\frac{E\phi_n}{1-\nu^2}}. \tag{4}$$

The significance of K_0 is that pure mode-I crack growth in a homogeneous elastic solid with the given cohesive properties takes place at $K_I/K_0 = 1$ [32]. Unless otherwise specified the cohesive properties were taken as $\sigma_{\text{coh}} = 0.5$ GPa and $\delta_n = 3b$ giving a work of fracture $\phi_n \approx 1.0$ J/m^2.

The effect of the formation of an oxide layer and the subsequent surface contact during unloading is modelled by specifying unloading from and reloading to the monotonic cohesive law as discussed in Refs. [23–25]. We emphasize that the irreversibility in the cohesive relation does not alter the cohesive strength.

For purposes of characterizing the tensile properties of the materials, results will also be

presented for a tensile bar shown in Fig. 3a with the slip systems making angles $\alpha = \pm 30°$ and 90° with the tensile axis of the specimen. The origin of the coordinate system is placed such that the bar occupies $0 \leq x_1 \leq W$ and $-H \leq x_2 \leq H$. With symmetry about the x_1-axis assumed, the region $x_2 \geq 0$ is analyzed. A displacement rate $\dot{U}$ and shear free conditions are prescribed on the edge where the loading is imposed,

$$\dot{u}_2 = \dot{U},\ \dot{T}_1 = 0 \quad \text{on } x_2 = H,$$

where $\dot{(\ )}$ denotes time differentiation.

The lateral sides are traction free

$$\dot{T}_1 = \dot{T}_2 = 0 \quad \text{on } x_1 = 0, W,$$

and symmetry conditions on the center-line are given by

$$\dot{u}_2 = 0,\ \dot{T}_1 = 0 \quad \text{on } x_2 = 0.$$

The overall stress σ is computed as

$$\sigma = \frac{1}{W}\int_0^W T_2(x_1, H)\mathrm{d}x_1.$$

All calculations presented here were carried out on a tensile bar $2H \times W = 16 \times 4$ μm and at the imposed loading rate $\dot{U}/H = 100/\mathrm{s}$. The discrete dislocation plasticity predictions of the tensile response are not sensitive to the specimen size [25].

The plane strain tensile response of materials (i)–(iv), with the source and obstacle strengths mentioned previously, is shown in Fig. 3b. In each case, the stress versus strain behavior is linear up to a yield strength and then the overall behavior is essentially nonhardening with fluctuations associated with the relatively small specimen size. The value of the yield strength, denoted by σ_Y, is identified with the stress at $\varepsilon = 0.001$. For material (i) $\sigma_Y = 60$ MPa, for material (ii) $\sigma_Y = 30$ MPa, for material (iii) $\sigma_Y = 25$ MPa and for material (iv) $\sigma_Y = 20$ MPa. Subsequently, each material is referred to by the value of its yield strength.

3. Scaling with yield strength

First, for comparison purposes, we present calculations carried out with K_I monotonically increasing. The computed curves of K_I versus crack advance, Δa, are shown in Fig. 4a for the four materials. For the three lowest yield strength materials, crack growth initiates with $K_I < K_0$. The

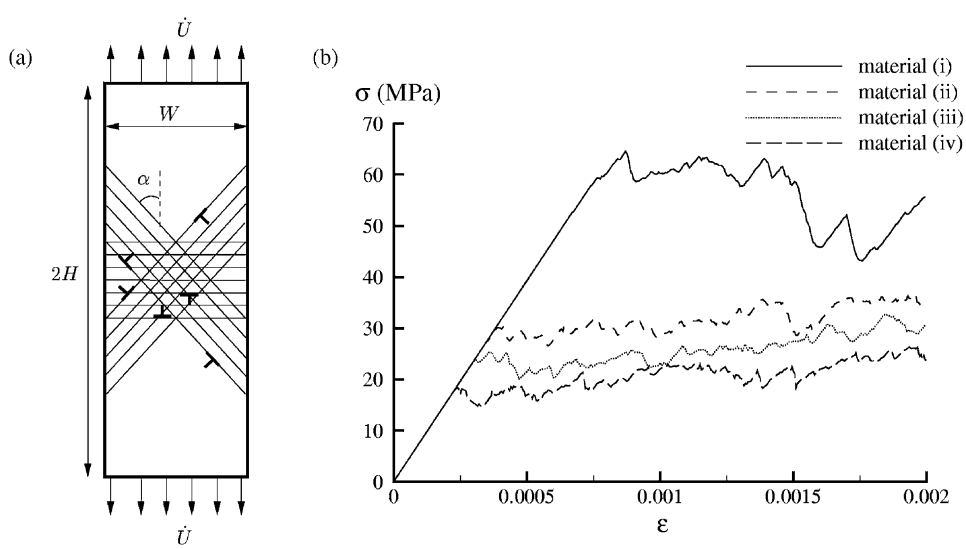

Fig. 3. (a) Sketch of the boundary value problem analyzed to obtain the tensile stress versus strain response of the uncracked single crystal. (b) Tensile stress versus strain curves for the four sets of nucleation and obstacle strengths used in the small scale yielding calculations with $E = 70$ GPa.

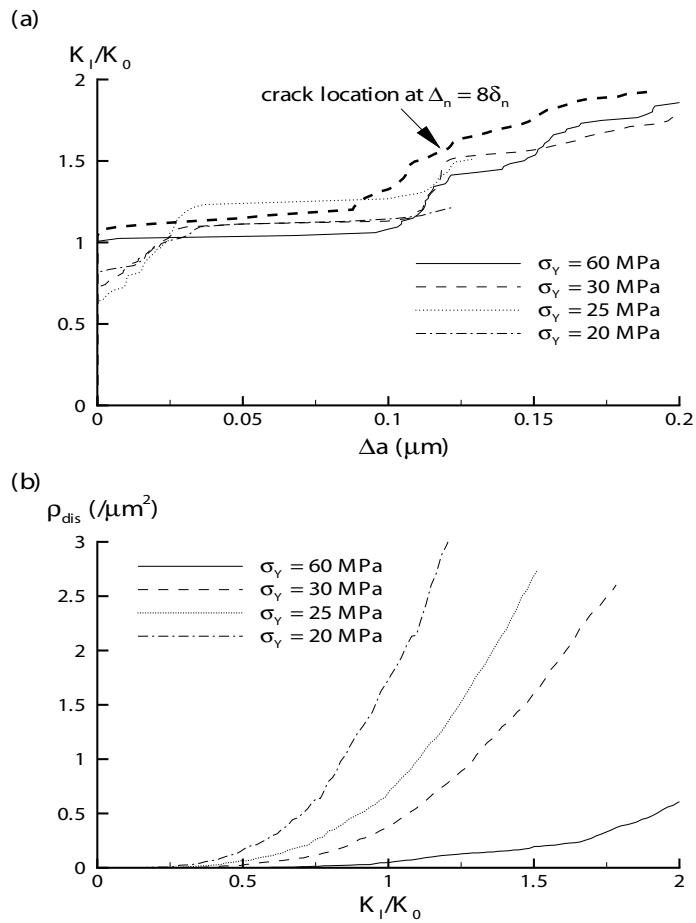

Fig. 4. (a) K_I/K_0 versus crack extension Δa for monotonic loading of four single crystals with $E = 70$ GPa and with values of yield strength σ_Y as indicated. The crack extension, Δa, is measured using the furthest point from the initial crack tip where $\Delta_n = 4\delta_n$. For comparison purposes, the response with $\sigma_Y = 30$ MPa is also shown (thicker line) using $\Delta_n = 8\delta_n$ to identify the crack location. (b) The evolution of the dislocation density with increasing K_I/K_0 for the above four cases.

location of the current crack tip is defined as the furthest point from the initial crack tip where Δ_n exceeds $4\delta_n$ (=3 nm in the calculations here). With a low value of mean nucleation strength, τ_{nuc}, dislocations nucleate very early in the deformation history and the stresses from such dislocations in the near crack tip region lead to opening of the cohesive surface before K_I reaches K_0. However, K_I increases rapidly during the very early stages of crack extension and reaches K_0 after only 0.04 μm (40 nm) of crack growth. The calculations were repeated using $\Delta_n \geq 8\delta_n$ to define the crack position. The K_I/K_0 versus Δa curve for the calculation with $\sigma_Y = 30$ MPa using $8\delta_n$ to define the crack location is shown in Fig. 4a. For crack extensions exceeding $\Delta a \approx 0.05$ μm, the monotonic K_I/K_0 versus Δa curves are not sensitive to which definition of crack position is used, which is consistent with previous crack growth studies using a cohesive formulation, see for example Ref. [33]. Similar differences were seen for the other values of σ_Y. In all subsequent calculations, the crack position is defined at $\Delta_n = 4\delta_n$. For both definitions of crack location, the crack growth resistance is rather independent of σ_Y for crack extensions up to $\Delta a \approx 0.2$ μm.

The evolution of the dislocation density, ρ_{dis} (number of dislocations per unit area of the process

window), with increasing applied K_I is shown in Fig. 4b for each of the four materials. Although ρ_{dis} with $\sigma_Y = 20$ MPa is about a factor of 10 higher than for σ_Y=60 MPa, the monotonic crack growth resistance is not sensitive to the value of the yield strength. This is a consequence of the dual role dislocations play in the fracture process, as discussed by Cleveringa et al. [34]. On the one hand, local stress concentrations associated with discrete dislocations near the crack tip together with the stress concentration associated with the crack itself cause the crack to propagate. On the other hand, plasticity caused by the motion of the dislocations increases the resistance to crack growth and tends to arrest the crack. The stress concentrations due to dislocations near the crack tip dominate and the crack growth behavior is relatively independent of the yield strength and dislocation density. Indeed, it is the stress concentration due to the near crack-tip dislocation structure that gives rise to fracture in these calculations. Here, $\sigma_{coh}/\sigma_Y = 8.33$ for $\sigma_Y = 60$ MPa, $\sigma_{coh}/\sigma_Y = 16.7$ for $\sigma_Y = 30$ MPa, $\sigma_{coh}/\sigma_Y = 20$ for $\sigma_Y = 25$ MPa and $\sigma_{coh}/\sigma_Y = 25$ for $\sigma_Y = 20$ MPa. For a nonhardening solid, conventional continuum plasticity predicts that crack growth is essentially precluded for $\sigma_{coh}/\sigma_Y > 4$, Ref. [35].

Next, cyclic loading with the remote applied stress intensity factor varying between K_{min} and K_{max} is considered. The ratio $R = K_{min}/K_{max}$ and the difference $\Delta K_I = K_{max} - K_{min}$ are used to characterize the cyclic loading; in all cyclic calculations here $R = 0.3$. To determine the fatigue threshold, calculations are carried out starting at some ΔK_I and then reducing ΔK_I until a cycle-by-cycle crack growth rate $da/dN \leq 10^{-3}$ μm/cycle is obtained. The fatigue threshold is then defined as the mean of the last two values of ΔK_I, cf. Ref. [23]. Typically, steps of $\Delta K_I/K_0 = 0.05$ are used. Crack advance versus time curves for the near-threshold values of applied $\Delta K_I/K_0 = 0.83$ for $\sigma_Y = 60$ MPa and $\Delta K_I/K_0 = 0.78$ for $\sigma_Y = 30$ MPa and $\sigma_Y = 25$ MPa are shown in Fig. 5a. In all cases there is an initial "burst" of crack growth during the first loading cycle with the crack growth rate subsequently settling down to a steady cycle-by-cycle growth rate $da/dN \approx 10^{-3}$ μm/cycle after about the third cycle as shown in the insert in Fig. 5a. It is worth emphasizing that continued crack growth occurs

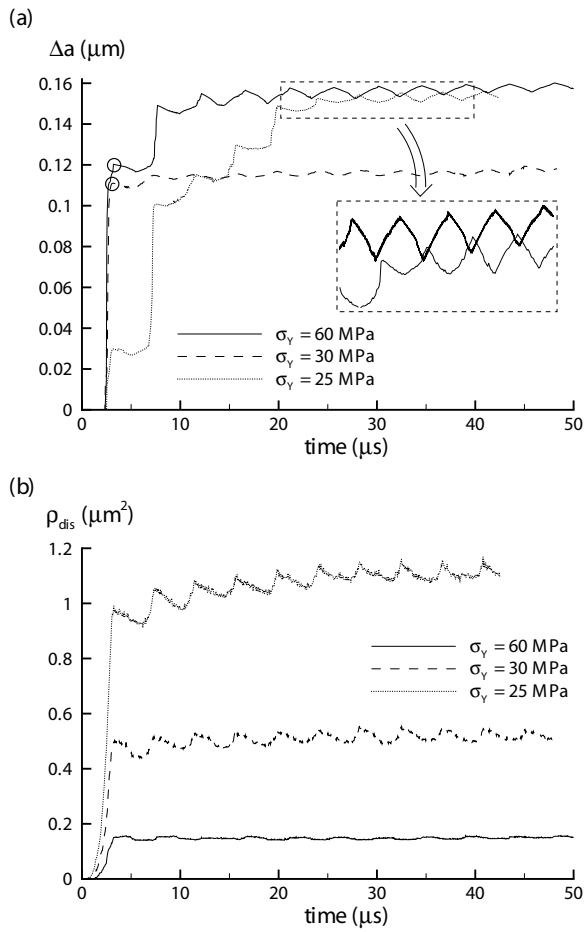

Fig. 5. (a) Time evolution of the crack extension Δa (the insert shows a more detailed view of the evolution of the crack extension) and (b) time evolution of the dislocation density for three single crystals (E = 70 GPa) identified via their yield strengths at the near-threshold values of $\Delta K_I/K_0$ with $R = 0.3$. For $\sigma_Y = 60$ MPa $\Delta K_I/K_0 = 0.83$, while $\Delta K_I/K_0 = 0.78$ in the other two cases.

under cyclic loading for a value of K_{max} at which the crack would have arrested under monotonic loading, see Fig. 4a. Fig. 5b shows the time evolution of dislocation density for the three loading cases shown in Fig. 5a. The dislocation density increases gradually with the number of loading cycles: as in Refs. [23–25], it is the evolving dislocation structure that gives rise to cycle-by-cycle crack growth. Furthermore, for approximately equal values of applied ΔK_I, the three materials in Fig. 5 exhibit approximately equal cycle-by-cycle

crack growth rates even though the number of dislocations (or the dislocation density) is about a factor of six higher with σ_Y = 25 MPa than with σ_Y = 60 MPa.

Fig. 6 shows contours of σ_{22} and the dislocation distributions in a region near the crack tip for the calculations with σ_Y = 60 MPa and with σ_Y = 30 MPa at the loading stages marked by the circles in Fig. 5a. These points are at the first load peak and the values of K_{max}/K_0 are 1.19 and 1.1 for σ_Y = 60 MPa and σ_Y = 30 MPa, respectively. While the number of dislocations with σ_Y = 60 MPa (Fig. 6a) is less than with σ_Y = 30 MPa (Fig. 6b), the values of the opening stress σ_{22} near the crack tip are nearly the same. Thus, as under monotonic loading conditions, the stress concentrations of the dislocations dominate the near crack tip stress field, which results in crack tip stresses (and crack growth rates) that are rather independent of the yield strength of the material. The crack opening profiles (shown below the x_1-axis with the displacements magnified by a factor of 10) show greater crack tip blunting with σ_Y = 30 MPa.

The results of all the fatigue threshold calculations carried out with various yield strengths, normalized by Young's modulus, are summarized in Fig. 7. The effective stress intensity range ΔK_I^{eff} is defined by [23,24]

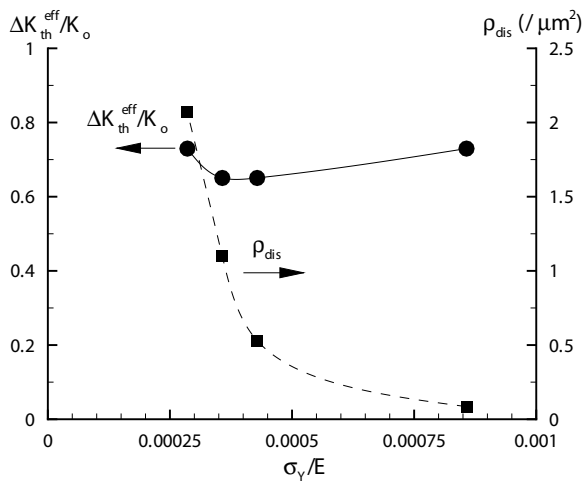

Fig. 7. Normalized effective fatigue threshold $\Delta K_{th}^{eff}/K_0$, (R = 0.3), as a function of the normalized yield strength σ_Y/E for single crystals with E = 70 GPa. The corresponding dislocation densities at first load peak for threshold values of applied ΔK_I are also shown.

$$\Delta K_I^{eff} = \begin{cases} K_{max} - K_{op} & \text{for } K_{min} < K_{op} \\ \Delta K_I & \text{for } K_{min} \geq K_{op} \end{cases}, \quad (5)$$

Here, K_{op} is the value of K_I at which the crack starts to open upon reloading. As in Refs. [23,24], $K_{cl} \approx K_{op}$ where K_{cl} is the value of K_I at complete closure. The figure also shows the corresponding

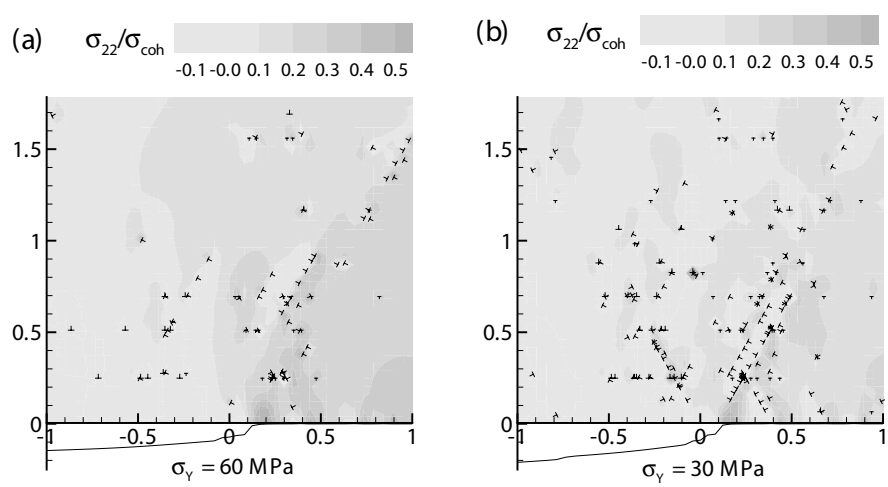

Fig. 6. Distribution of dislocations and opening stress σ_{22}/σ_{coh} in the neighborhood of the crack tip at the first load peak as marked with circles in Fig. 5a. (a) σ_Y = 60 MPa and (b) σ_Y = 30 MPa. The crack tip profiles with displacements magnified by a factor of 10 are shown below the x_1-axis in each case.

dislocation densities at the first load peak. The computed values of $\Delta K_{th}/K_0$ are approximately 0.84, 0.78, 0.77 and 0.82, for σ_Y = 60, 30, 25 and 20 MPa, respectively, while the corresponding values of $\Delta K_{th}^{eff}/K_0$ shown in Fig. 7 are 0.73, 0.65, 0.65 and 0.73. The effective fatigue threshold is essentially independent of yield strength despite the fact that the dislocation densities at the first load peak for these threshold values of ΔK_I increase substantially with decreasing yield strength.

In order to investigate the variation of crack growth rate with yield strength, cyclic loading calculations were carried out for values of applied ΔK_I (R = 0.3) greater than the threshold value with σ_Y = 60 and 30 MPa. In each calculation, 8–10 cycles were computed and the crack growth per cycle, da/dN, is taken as the average crack advance per cycle. The results from these computations are summarized in Fig. 8. The log(da/dN) versus log($\Delta K_I/K_0$) curves show two distinct regimes. In the first regime, the average crack growth per cycle is smaller than a lattice spacing with the crack either remaining stationary or growing at an undetectable rate below a threshold value ΔK_{th}. Just above the threshold, da/dN increases sharply with ΔK_I. Subsequently, there is a "knee" in the log(da/dN) versus log($\Delta K_I/K_0$) curve with da/dN increasing more gradually with increasing ΔK_I corresponding to a regime approaching Paris law [2] behavior. The log(da/dN) versus log($\Delta K_I/K_0$) curves are similar for the calculations with σ_Y = 60 and 30 MPa, indicating that the fatigue crack growth rate is not sensitive to yield strength in the lower Paris law regime as well. The crack growth rates as a function of the effective stress intensity factor range ΔK_I^{eff} are also shown in Fig. 8 with the curves again reasonably independent of the yield strength of the material. Indeed, the crack growth rates beyond the "knee" whether plotted against ΔK_I or ΔK_I^{eff} are less sensitive to yield strength than is the fatigue threshold. Results are not shown for σ_Y = 25 and 20 MPa because the high dislocation densities that developed made the computing times too long to continue those calculations into the Paris law regime.

4. Scaling with Young's modulus

The plane strain tensile response of two materials identical to the material with σ_Y = 60 MPa, material (i), but with Young's moduli E = 140 and 35 GPa (Poisson's ratio ν = 0.33) are shown in Fig. 9. For comparison purposes, the response of material (i), E = 70 GPa, from Fig. 3b is also shown. It is seen that the predicted yield strength is reasonably independent of Young's modulus E with all other properties fixed.

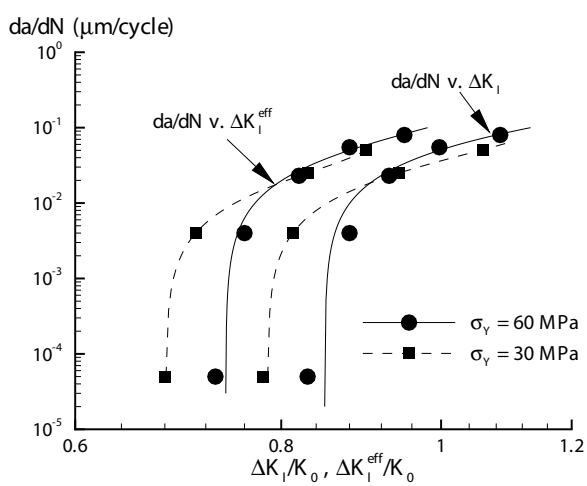

Fig. 8. The cyclic crack growth rate da/dN versus $\Delta K_I/K_0$ and $\Delta K_I^{eff}/K_0$, (R = 0.3), for the mode I cyclic loading of single crystals with E = 70 GPa and with σ_Y = 60 MPa and σ_Y = 30 MPa.

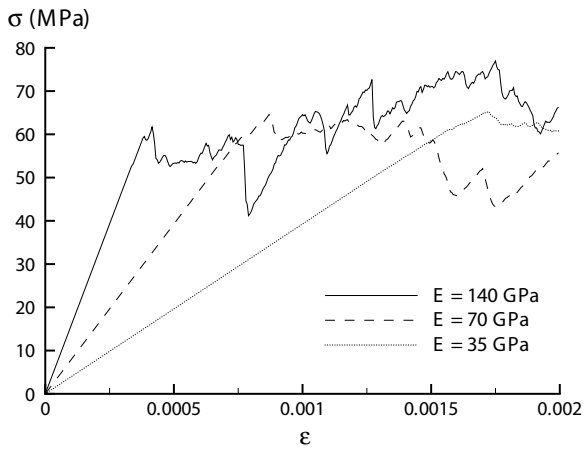

Fig. 9. Tensile stress versus strain curves with three values of Young's modulus E. The mean nucleation source strength τ_{nuc} = 50 MPa and obstacle strength τ_{obs} = 150 MPa in all three calculations.

At least from the perspective of a conventional continuum plasticity framework, three material parameters with the dimension of stress characterize the response: Young's modulus E, the flow strength σ_Y and the cohesive strength σ_{coh}. From these, three dimensionless groups can be formed, two of which are independent, for example, σ_{coh}/σ_Y, E/σ_{coh} and σ_Y/E. In addition, the fracture behavior is governed by $\phi_n = \exp(1)\sigma_{coh}\delta_n$ as well as by σ_{coh} so that three fracture property related dimensionless groups are $\phi_n/(\sigma_Y b)$, E/σ_{coh} and δ_n/b. Of these five dimensionless groups, only three are independent.

In the previous section, the effect of σ_Y/E has been studied by varying σ_Y with constant E = 70 GPa and fixed cohesive properties. Here, the variation of the fatigue threshold with Young's modulus is investigated with σ_Y fixed at ≈60 MPa, by keeping the properties of sources and obstacles the same as for material (i). Simultaneously we vary cohesive properties so that: (1) δ_n/b and $\phi_n/(\sigma_Y b)$ are fixed; (2) E/σ_{coh} and $\phi_n/(\sigma_Y b)$ are fixed; and (3) δ_n/b and E/σ_{coh} are fixed. Relative to the reference values

$$E/\sigma_{coh} = 140,\ \phi_n/(\sigma_Y b) = 68,\ \delta_n/b = 3,\ \sigma_{coh}/\sigma_Y = 8.33,\ \sigma_Y/E = 0.00085,$$

the following variations are considered for each of the three cases:

1. Young's modulus varying between E = 35 and 140 GPa with the cohesive properties fixed. Thus, σ_{coh}/σ_Y is unchanged, and both E/σ_{coh} and σ_Y/E vary.
2. Young's modulus varying in the same range as in (1), but with concomitant variations of σ_{coh} and $\delta_n/b \propto \sigma_{coh}^{-1}$ so that E/σ_{coh} = 140 and the cohesive surface energy remains fixed. This case corresponds to a set of cohesive surfaces with $\phi_n \approx 1.0$ J/m^2 and cohesive strengths varying between σ_{coh} = 0.25 and 1.0 GPa.
3. Young's modulus varying between E = 47 GPa (E < 47 GPa resulted in brittle fracture with minimal dislocation activity) and E = 140 GPa with variations of σ_{coh} and $\phi_n \propto \sigma_{coh}$ so that E/σ_{coh} = 140 while δ_n/b = 3. Thus, σ_{coh}/σ_Y and $\phi_n/(\sigma_Y b)$ vary. This case corresponds to a set of cohesive surfaces with σ_{coh} varying between 0.34 and 1.0 GPa and ϕ_n varying between 0.67 and 2.0 J/m^2.

The ranges of variation are summarized in Table 1 including the analyses in Section 3 where σ_Y was varied which is labeled case (0). Case (3) is identical, in terms of the nondimensional groups relevant in conventional continuum plasticity, to case (0) but the variations have a different origin and, therefore, span a somewhat different range.

Qualitatively, the near-threshold crack growth behavior is similar to that described in Section 3 so that here only the results for the values of the effective fatigue threshold ΔK_{th}^{eff} at R = 0.3 are summarized.

Fig. 10a shows that the values of $\Delta K_{th}^{eff}/K_0$ are nearly the same in all nine calculations, with some variation for the lowest strength materials (σ_Y/E < 0.0005). Thus, our calculations predict that ΔK_{th}^{eff} scales with K_0 to a good degree of approximation. From Eq. (4), $K_0 \propto \sqrt{E\phi_n}$. Hence, in case (1) and case (2), where ϕ_n is fixed, this scaling implies $K_0 \propto \sqrt{E}$. On the other hand in case (3), $\phi_n \propto \sigma_{coh} \propto E$ implies that $K_0 \propto E$. To further explore the scaling with E, the effective fatigue threshold ΔK_{th}^{eff} normalized by $E\sqrt{b}$ is plotted in Fig. 10. In Fig. 10b, the slope of the linear fit to case (1) is

Table 1
Summary of variations of nondimensional groups considered in Section 3, labeled case (0), and cases (1)–(3) analyzed in Section 4

Case	E/σ_{coh}	$\phi_n/(\sigma_Y b)$	δ_n/b	σ_{coh}/σ_Y	σ_Y/E
(0)	140	68–204	3	8.33–25	0.00029—0.00085
(1)	70–280	68	3	8.33	0.00042—0.0017
(2)	140	68	1.5–6	4.2–16.7	0.00042—0.0017
(3)	140	46.5–136	3	5.7–16.7	0.00042—0.0013

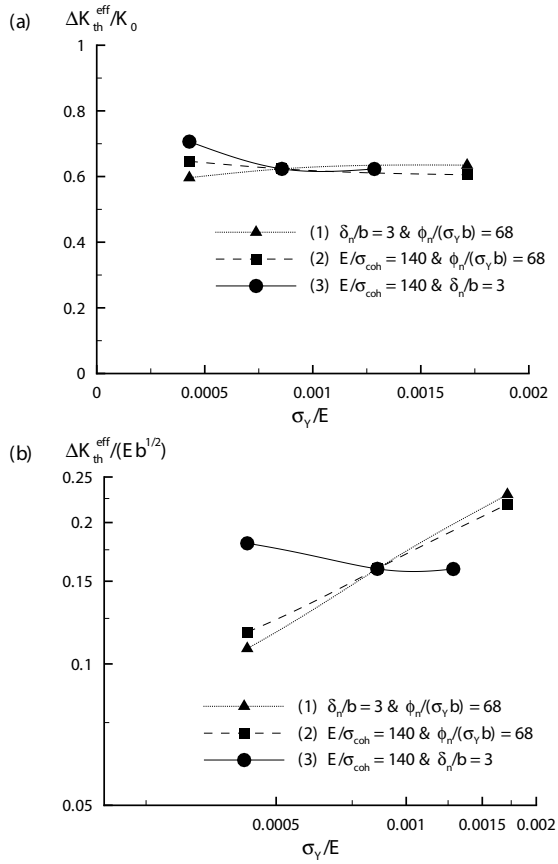

Fig. 10. The effective fatigue thresholds (a) $\Delta K_{th}^{eff}/K_0$ and (b) $\Delta K_{th}^{eff}/E\sqrt{b}$ at $R = 0.3$ as a function of normalized yield strength σ_Y/E. Three cases with the yield strength fixed at $\sigma_Y \approx 60$ MPa are shown: (1) fixed cohesive properties, $\delta_n/b = 3$ and $\phi_n/(\sigma_Y b) = 68$ (2) a fixed cohesive energy $\phi_n/(\sigma_Y b) = 68$ and the cohesive strength ratio $E/\sigma_{coh} = 140$ and (3) fixed cohesive strength ratio $E/\sigma_{coh} = 140$ and cohesive displacement $\delta_n/b = 3$.

0.55 and the slope of the linear fit to case (2) is 0.45. Thus, there is good accord with the ideal square root scaling. For case (3), the deviation from linear scaling with E at a low value of σ_Y/E is seen.

Presuming that the cohesive strength of crystalline metals scales with E and that the cohesive displacement at which the cohesive strength is attained, δ_n, and the Burgers vector b both scale similarly with lattice spacing, the experimentally observed linear scaling with E in Refs. [5,6] emerges in our calculations from $\Delta K_{th}^{eff} \propto K_0$. Our

calculations also predict that a deviation from the linear scaling is expected for very low strength materials.

5. Discussion

The scaling that emerges from our calculations for ΔK_{th}^{eff} is: (i) that it is nearly independent of the tensile flow strength and (ii) that it scales with $\sqrt{E\phi_n}$ where $\phi_n = \exp(1)\sigma_{coh}\delta_n$ is the cohesive energy. Variations in σ_{coh} and δ_n individually do not have a significant effect on the predicted fatigue threshold as long as their product, ϕ_n, is kept fixed (Fig. 10a). This scaling holds over ranges of yield strengths, cohesive strengths and elastic moduli varying by factors of three to four. From a continuum plasticity perspective, it is surprising that varying the ratio σ_{coh}/σ_Y between $\approx$6 and 25 has little effect on the predicted fatigue threshold. When comparing different materials and presuming that $\sigma_{coh} \propto E$ and $\delta_n \propto b$, the scaling implies that $\Delta K_{th}^{eff} \propto E\sqrt{b}$. On the other hand, for a fixed material, but with varying cohesive energy, due for example to chemical effects [36,37], $\Delta K_{th}^{eff} \propto \sqrt{\phi_n}$. We also find that varying the flow strength by a factor of two has no effect on the predicted crack growth rate in the lower Paris law regime.

In the models of Pippan et al. [17–19] and Wilkinson et al. [20], fatigue crack growth is assumed to be deformation governed with the fatigue threshold corresponding to the nucleation of a dislocation from the crack tip or a source near the crack tip. Assuming that dislocation emission occurs from the crack tip at a critical k_{emit}, Wilkinson et al. [20] analyzed mode II fatigue crack growth and found that ΔK-governed fatigue crack growth occurs when $\Delta K_{th} \approx 1.1 k_{emit}$. Using estimates from [22,38] for Cu, $k_{emit} \approx 0.10 - 0.12E\sqrt{b}/(1 + \nu)$, $\Delta K_{th} \approx 0.075 - 0.95E\sqrt{b}$.[1] Thus, the scaling is the same as in the calculations here although the physical mechanism is different—dislocation emission in Refs. [19,20] and decohesion here. It is worth noting that the models in Refs. [19,20] do not actually calculate crack growth but specify the crack growth rate in terms of the number of Burgers vectors emitted per cycle (one per cycle at the threshold) and are restricted to cyclic loading. As a consequence, investigation of the effect of variations in the tensile yield strength on the fatigue threshold are outside the scope of such models. Furthermore, such models neglect the contributions of dislocations nucleated away from the crack tip to the crack tip stress field and to the plastic dissipation.

In our analyses, dislocations nucleate from Frank–Read sources distributed throughout the material. There is no special nucleation from the crack tip. In principle, dislocation nucleation from the crack tip via a Peierls mechanism can also be incorporated into the current framework by employing a cohesive relation of the type suggested by Beltz and Rice [39]. This would permit an analysis of the circumstances under which fatigue crack growth would occur by cleavage or by dislocation emission from the crack tip.

As in Refs. [23–25], the fracture behavior in the present study is an outcome of the interplay between the cohesive and plastic flow properties. Under both monotonic and cyclic loading conditions, decohesion occurs in the presence of plastic deformation because of the high local stress concentrations ahead of the crack that arise from the near-tip dislocation structures. For ductile metals under monotonic loading conditions, cleavage-like separation in the presence of plastic flow is rarely, if ever observed. On the other hand, under cyclic loading conditions, cleavage-like fracture modes are observed in ductile metals in the near-threshold and short crack regimes, Refs. [1; p. 348], [40,41]. Presumably, under monotonic loading continued crack tip blunting occurs and the reduction in stress concentration due to the change in crack tip geometry (not accounted for in the small geometry change analyses here) precludes cleavage. However, under cyclic loading conditions, because of the evolving near crack tip dislocation structures, stress levels progressively increase with the crack remaining relatively sharp.

[1] To compare with Ref. [19], we used the values given of $\theta = 70°$ and $\Phi = 0°$ in their Eq. (1) and data from their Table 1 and obtained a value for their predicted ΔK_{th} for Al comparable to the values we obtain, but the value of ΔK_{th} displayed in Table 1 of Ref. [19] is about a factor of two greater.

Hence, progressive cleavage-like separation occurs. Well into the Paris regime, where larger scale plastic flow takes place, the deformation governed mechanisms [10,21], often assumed to govern fatigue crack growth may in fact become more prominent. Indeed, a transition from a cleavage-like fracture mode to a ductile fracture mode with increasing ΔK and K_{max} was seen in Ref. [41].

Conventional continuum plasticity models predict that fatigue crack growth is sensitive to the value of the yield strength, see e.g. Ref. [1; p. 346]. This is because conventional continuum plasticity describes the stress relaxation associated with the motion of dislocations but not the stress enhancement associated with the organized dislocation structures that form near the crack tip. The results here and in Refs. [22–25] indicate that the stress enhancement aspect plays a dominant role in the near-threshold regime and for short cracks. With ratios of σ_{coh}/σ_Y in the range 8–25 for a nonhardening solid, conventional continuum plasticity would predict that crack growth is precluded under the circumstances analyzed. The present results indicate that the observed relative lack of dependence of the fatigue threshold in ductile metals on yield strength and the observed scaling with Young's modulus can emerge as consequences of a cleavage-like fracture mode (as often observed in the near-threshold regime, e.g. Refs. [1; p. 348] [40,41]) coupled with the stress concentration arising from near crack tip organized dislocation structures.

Results for ΔK_{th}^{eff} from all the calculations reported in this study are summarized in Fig. 11 in a form similar to the experimental results in Fig. 1. On a scale similar to that in Fig. 1, our calculations also show that $\Delta K_{th}^{eff}/E$ is reasonably independent of the normalized strength σ_Y/E over approximately a decade. In our calculations $\Delta K_{th}^{eff}/E \approx 1.6 \times 10^{-6} - 3.2 \times 10^{-6}\sqrt{m}$, which is significantly below the main body of data in Fig. 1. However, it worth noting that it is within the spread of data in Fig. 1 for higher strength Al alloys.

In the calculations reported here $\Delta K_{th}^{eff}/E\sqrt{b} \approx 0.1-0.2$ which is a factor of five to ten smaller than in the experiments reported in Refs. [5,6] and the experimental data plotted in Fig. 1. These predictions are however about a factor of two greater than for the model of Wilkinson et al. [20]. There are several possible reasons for the discrepancy with experiment: (i) the high loading rate employed to reduce computational time acts to reduce the amount of plastic dissipation [30]; (ii) effects of crack tip blunting are not taken into account in this small-strain analyses; (iii) the calculations are plane strain with the entire crack front growing simultaneously; and (iv) the analyses are carried out for small amounts of pure mode-I crack growth in a single crystal while in most experiments the threshold is inferred from experiments on polycrystalline metals with large amounts crack growth with mixed-mode loading effects due to off-plane crack growth and interaction with grain boundaries. It is possible that when complex crack paths and grain boundary effects come into play that plastic dissipation, and hence the material's flow strength, has a greater effect on the average fatigue crack growth rate. However, it should be emphasized that the discrete dislocation and the cohesive framework presented here can be extended and can model polycrystalline materials and crack growth off the initial crack plane, albeit at an increased computational cost.

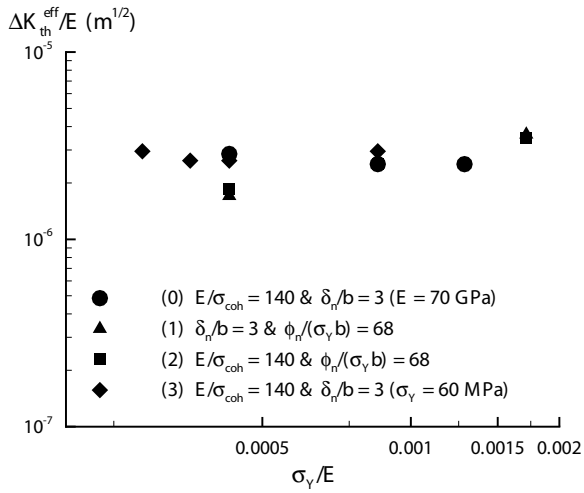

Fig. 11. ΔK_{th}^{eff} for all the calculations reported in this study and plotted in the form of Fig. 1. The data shows that similar to experiment, ΔK_{th}^{eff} is approximately independent of the yield strength σ_Y and scales approximately linearly with Young's modulus E.

6. Conclusions

We have carried out analyses of fatigue crack growth in single crystals under remote mode I plane strain conditions. Plastic flow arises from the collective motion of large numbers of discrete dislocations and the fracture properties are embedded in a cohesive surface constitutive relation. Material properties were varied so that values of flow strength differing by a factor of three, values of Young's modulus differing by a factor of four, values of cohesive strength differing by a factor of four and values of cohesive energy differing by a factor of three were considered.

- The effective fatigue threshold $\Delta K_{\text{th}}^{\text{eff}}$ is proportional to the cohesive strength as measured by K_0 in Eq. (4) with some deviation occurring for very low strength materials.
- With the values of cohesive strength, cohesive energy and Young's modulus fixed, $\Delta K_{\text{th}}^{\text{eff}}$ is seen to be approximately constant for flow strengths varying by a factor of three.
- With the values of cohesive strength, cohesive energy and Young's modulus fixed, varying the value of the flow strength by a factor of three gives rise to crack growth rates in the lower Paris law regime that are independent of yield strength whether plotted against ΔK_I or ΔK_I^{eff}.
- With the yield strength fixed and with the ratios of cohesive strength to Young's modulus and cohesive length to Burgers vector fixed, the effective fatigue threshold $\Delta K_{\text{th}}^{\text{eff}}$ varies approximately linearly with Young's modulus. Deviation from this scaling is predicted for very low strength materials. With Young's modulus fixed, $\Delta K_{\text{th}}^{\text{eff}}$ is predicted to vary as the square root of the cohesive energy.
- The results here and in Refs. [23–25] show that the fatigue threshold, Paris law behavior, striations, the accelerated growth of short cracks as well as the observed scaling of the fatigue threshold and of fatigue crack growth rates in the near-threshold regime emerge naturally from a unified framework where plastic flow arises from the motion of large numbers of discrete dislocations and the fracture properties are embedded in a cohesive surface constitutive relation.

Acknowledgements

Support from the AFOSR MURI at Brown University on *Virtual Testing and Design of Materials: A Multiscale Approach* (AFOSR Grant F49620-99-1-0272) is gratefully acknowledged. We are pleased to acknowledge Prof. W.O. Soboyejo of Princeton University for insightful discussions during the course of this work. We are also grateful to Prof. N.A. Fleck of Cambridge University for providing the data for Fig. 1.

References

[1] Suresh S. Fatigue of materials. Cambridge, UK: Cambridge University Press, 1998.
[2] Paris PC, Gomez MP, Anderson WP. Trend Eng 1961;13:9.
[3] Minakawa K, McEvily AJ. Proc Int Conf Fatig Thresholds, Stockholm 1981;1:373.
[4] Liaw PK, Leax TR, Williams RS, Peck MG. Acta Metall 1982;30:1607.
[5] Liaw PK, Leax TR, Logsdon WA. Acta Metall 1983;31:1581.
[6] Hertzberg RW. Int J Fract 1993;64:R53.
[7] Kang KJ, Garton D, Fleck NA. CUED/C/MATS/TR.199. Cambridge Univ Eng Dept, UK. Internal report, 1992.
[8] Usami S, Shida S. Fatig Eng Mater Struct 1979;1:471.
[9] Donahue RJ, Clark HM, Atanmo P, Kumble R, McEvily AJ. Int J Fract 1972;8:209.
[10] Laird C, Smith GC. Phil Mag 1962;7:847.
[11] McClintock FA. Fracture 1971;3:47 (Liebowitz FA, editor).
[12] Weertman J. Int J Fract 1966;2:460.
[13] Rice JR. Fatigue crack propagation. ASTM STP 1967;415:247.
[14] Nguyen O, Repetto A, Ortiz M, Radovitzky RA. Int J Fract 2001;110:351.
[15] Tvergaard T, Hutchinson JW. Proc Int Conf Fatig, Stockholm 2002;1:107.
[16] Riemelmoser FO, Gumbsch P, Pippan R. Mat Trans 2001;42:2.
[17] Pippan R. Acta Metall Mat 1991;39:255.
[18] Riemelmoser FO, Pippan R. Mat Sci Eng A 1997;234-236:135.
[19] Riemelmoser FO, Pippan R, Stüwe HP. Acta Mat 1998;46:1793.
[20] Wilkinson AJ, Roberts SG, Hirsch PB. Acta Mat 1998;46:379.

[21] Neumann P. Acta Metall 1969;17:1219.
[22] Rice JR, Thomson R. Phil Mag 1974;29:73.
[23] Deshpande VS, Needleman A, Van der Giessen E. Acta Mat 2001;49:3189.
[24] Deshpande VS, Needleman A, Van der Giessen E. Acta Mat 2002;50:831.
[25] Deshpande VS, Needleman A, Van der Giessen E. Acta Mat 2003;51:1.
[26] Cleveringa HHM, Van der Giessen E, Needleman A. Int J Plast 1999;15:837.
[27] Van der Giessen E, Needleman A. Model Simul Mater Sci Eng 1995;3:689.
[28] Needleman A. J Appl Mech 1987;54:525.
[29] Kubin LP, Canova G, Condat M, Devincre B, Pontikis V, Bréchet Y. Solid State Phenomena 1992;23-24:455.
[30] Cleveringa HHM, Van der Giessen E, Needleman A. Mat Sci Eng A 2001;1-2:37.
[31] Rose JH, Ferrante J, Smith JR. Phys Rev Lett 1981;47:675.
[32] Rice JR. J Appl Mech 1968;35:379.
[33] Xu X-P, Needleman A. Mech Phys Solids 1994;42:1397.
[34] Cleveringa HHM, Van der Giessen E, Needleman A. J Mech Phys Solids 2000;48:1133.
[35] Tvergaard V, Hutchinson JW. J Mech Phys Solids 1992;40:1377.
[36] Jarvis EAA, Hayes RL, Carter EA. Chem Phys Chem 2001;1:55.
[37] Van der Ven A, Ceder G. Phys Rev B Rapid Commun 2003;67:060101.
[38] Ohr SM. Mat Sci Eng 1985;72:1.
[39] Beltz GE, Rice JR. Acta Metall 1992;40:321.
[40] Sinha V, Mercer C, Soboyejo WO. Mat Sci Eng 2000;A287:30.
[41] Mercer C, Shademan S, Soboyejo WO. J Mat Sci 2003;38:291.